Palomar *et al.*
Reproductive Biology and Endocrinology (2025) 23:57
https://doi.org/10.1186/s12958-025-01386-z

Reproductive Biology and Endocrinology

RESEARCH

Open Access

Predictive potential of combined secretomics and image-based morphometry as a non-invasive method for selecting implanting embryos

Andrea Palomar[1†], Roberto Yagüe-Serrano[1†], Juan Vicente Martínez-Sanchis[2], Ignacio Iniesta[2], Alicia Quiñonero[1], Pedro José Fernández-Colom[2], Ana Monzó[2], José María Rubio[2], Inmaculada Molina[2] and Francisco Domínguez[1,3,4*]

Abstract

Background Non-invasive selection of human embryos for in vitro fertilization purposes is still a major challenge to pursue. Therefore, this study aims to identify non-invasive morphometric and secretomic parameters that reliably select the embryos with the highest likelihood of implantation prior to embryo transfer (ET).

Methods Prospective single-centre cohort study. Thirty-two day 5 blastocysts derived from 28 couples undergoing intracytoplasmic sperm injection (ICSI) and ET between January 2023 and April 2023. Patients were split according to their implantation outcome, confirmed with serum beta-human chorionic gonadotropin (b-hCG) levels > 5 mIU/mL nine days post-SET. Ninety-two proteins involved in embryonic developmental programming were measured in spent blastocyst media (SBM) using a protein extension assay. Sparse PLS-DA (sPLS-DA) was used for principal component analysis. Forty-seven morphometric parameters related to the trophoblast, inner cell mass and blastocele dimension were evaluated in microphotographs of day 5 embryos with ImageJ software.

T-test and Mann–Whitney tests were respectively used to compare morphometric measurements and normalized expression of secreted protein (NPx) levels between embryos that implanted or not. Predictive value of models of implantation based on embryo morphometric parameters and secreted proteins.

Results Chi-squared tests showed no significant differences in transferred blastocyst stage, quality, and state between subgroups. Implanting blastocysts ($n = 14$) presented significantly different morphometric shape descriptors (i.e., internal circularity, internal roundness, internal axis ratio, internal angle and trophoblast mean width) than non-implanting blastocysts ($n = 13$). Among the quantifiable proteins (86/92) in SBM from eleven implanting and nine non-implanting blastocysts, NPx and sPLS-DA analysis revealed three differentially expressed proteins. Matrilin-2 (MATN2) and legumain (LGMN) were significantly elevated ($p < 0.01$ in both cases) while thymosin beta-10 (TMSB10) was significantly decreased ($p < 0.05$) in implanting embryos. Predictive models based exclusively on morphometric or secreted protein profiles accurately discriminated implantation outcomes (AUC > 0.71). The model integrating

[†]Andrea Palomar and Roberto Yagüe-Serrano contributed equally to this work and should be regarded as joint first authors.

*Correspondence:
Francisco Domínguez
Francisco.Dominguez@ivirma.com
Full list of author information is available at the end of the article

the blastocysts' internal circularity, internal roundness, internal axis ratio and the NPx of MATN2 and TMSB10 in SBM had exceptional negative and positive predictive power for implantation outcomes (100% and 90.91%, respectively; AUC = 0.93).

Conclusions Morphometric shape descriptors and NPx levels of MATN2 and TMSB10 in SBM emerge as promising candidate markers for non-invasive embryo selection.

Keywords Non-invasive markers, Embryo morphometrics, Secretomic profile, Human embryos, Implantation potential

Introduction

Predicting embryo parameters to select blastocysts with the highest likelihood to implant, establish an ongoing pregnancy, and ultimately, lead to a live birth is a major ongoing challenge in assisted reproduction technologies.

Embryo culture media provides reliable information about the embryo's implantation potential [1, 2]. Diverse studies investigating secreted markers in conditioned embryo culture media found that certain compounds such as human chorionic gonadotropin (hCG) [3], lipoprotein A1 [4], histocompatibility antigen, class I, G (HLA-G) [5] and pregnancy-specific b-1 glycoprotein [6] might be associated with embryo quality and developmental potential. More recently, efforts to improve non-invasive embryo selection strategies have combined secreted markers with morphokinetic parameters [7–9]. However, most of these studies were focused on the presence of metabolites, such as lipids [10, 11], or the oxidative status of the culture media [7]. Some clinical studies leveraged the cell-free DNA in embryo culture media, which is highly concordant with preimplantation genetic testing results, to non-invasively predict embryo ploidy [12–14], disorders as β-thalassemia [15] or causes of miscarriage [16]. Despite these promising applications, notable technical flaws of this DNA analysis include putative maternal contamination from residual cumulus cells or DNA degradation [12].

Understanding the cell proteome is useful for tracking the physiological status of the cell [17]. The secretome, which includes proteins secreted or consumed by the embryo can be a source of non-invasive biomarkers. Classical secretomic techniques based on mass spectrometry have several disadvantages, such as their difficult interpretation and instrumentation, that hinders routine clinical implementation in reproductive medicine [18]. Emerging technologies combining immunoassay approaches with DNA-polymerase for proximity-depending polymerization (proximity extension assays, PEA) are gaining momentum due to their increased sensitivity and specificity, with a minimal quantity of sample required for multiplexing [19, 20]. In biomedicine, this immunoassay technology has been broadly used to detect unique protein profiles associated with various health conditions [21–28]. Even with evidence of PEA being applied for non-invasive embryo selection with [29, 30] or without [31] time-lapse embryo morphology assessments, the clinical potential of PEA technology in reproductive medicine is largely unexplored. Morphometric parameters can be very valuable to predict implantation potential. The embryo area, including the blastomeres and perivitelline space within plasma membrane, as well as zona pellucida thickness and blastomeres roundness, were significantly associated with successful implantation in cleavage-stage embryos [32, 33].

As time-lapse embryo culture data is not always available, the aim of the current study was to combine morphometric measurements of bright-field images taken at 5 days of development post-fertilization (blastocyst stage), just prior to embryo transfer with secreted markers in spent blastocyst culture medium (SBM) to provide an alternative and reliable non-invasive strategy to identify embryos with higher probabilities of reproductive success.

Methods

Ethical approval

This study was approved by the Ethical Research Board of the Polytechnic University Hospital La Fe (2018/0669). All participants provided written informed consent prior to their inclusion.

Study design

This prospective single-centre study included 32 human blastocysts (5 days post-fertilization) derived from couples undergoing either fresh or frozen embryo transfers after intracytoplasmic sperm injection (ICSI) cycles ($n = 30$) at the Assisted Reproduction Unit of the Hospital La Fe (Valencia, Spain) between January 2023 and April 2023. Female patients presenting adenomyosis, myomas or uterine fibroids, an endometrial thickness < 7 mm at the time of transfer were excluded from the study. Similarly, cycles with non-ejaculated sperm were excluded. Patients with hepatitis B/C or human immunodeficiency virus were also excluded from the study. Blastocysts

were either transferred in the same cycle or vitrified to be transferred in a subsequent cycle. Bright-field microphotographs and spent blastocyst media (SBM) were collected from each blastocyst prior to ET, for morphometric and secretomic analysis, respectively. Blastocysts were divided into two groups based on the implantation outcome.

Controlled ovarian stimulation, in vitro fertilization and embryo culture

Controlled ovarian stimulation protocols involved follicle stimulating hormone (FSH; dose range 1200–3000 IU; Gonal F, Merck) alone or in combination with human menopausal hormone (hMG; dose range 0–1500 IU; Ferring) or luteinizing hormone (LH; dose range 0 – 2100 IU; Menopur, Ferring). Ovulation was triggered with 500 IU human chorionic gonadotrophin (Ovitrelle, Merck) and/or a 0.25 mg GnRH antagonist (Orgalutran; MSD) when follicles surpassed a 16 mm diameter. Oocyte retrieval was performed 36 h later by ultrasound-guided vaginal aspiration.

Cumulus-oocyte complexes (COCs) were isolated and incubated for minimum three hours at 37°C and 5% CO_2 prior to enzymatic (in 1X hyaluronidase for under 60 s; 10-X Hyase, 90,176; Vitrolife) and mechanical denudation. Mature metaphase II (MII) oocytes were microinjected with a single motile spermatozoon selected using the swim-up technique. Fertilization was confirmed 16–18 h later, with the presence of two pronuclei. Zygotes were cultured in 20µL sequential culture medium (G-TL, 10,145, Vitrolife) until day 5 (blastocyst stage). Embryo staging and quality were assessed according to the ASEBIR criteria [34]. The SBM from each embryo was collected and stored at −80°C until further analysis.

Endometrial preparation and embryo transfer

Blastocysts were either transferred in the same cycle or cryopreserved for transfer in a subsequent cycle to ensure optimal endometrial conditions. Embryos were vitrified in open-pulled straws and thawed according to Kitazato protocols (VT601 and VT602, respectively). Intravaginal progesterone regimen (200 – 400 mg) was followed for endometrial priming to ensure correct embryo-endometrium synchrony in the case of frozen embryo transfers. On the same day of transference, cryopreserved embryos were thawed (VT602, Kitazato) and after post-thawing recovery, bright field images and SBM were collected prior embryo transfer. Finally, blastocysts were transferred using an ultrasound-guided catheter.

Reproductive outcome measures

The implantation, clinical pregnancy and live birth outcomes were recorded for all ETs. Successful implantation was defined as serum b-hCG levels > 5 mIU/mL nine days following ET. Clinical pregnancy was confirmed with serum b-hCG levels ≥ 10 IU/L, the presence of a gestational sac and fetal heartbeat detected by ultrasound within 12 weeks of pregnancy. Live birth was defined as the delivery of a live newborn after minimum 24 weeks of pregnancy.

Evaluation of embryo morphometrics

Morphometric parameters were assessed in bright field images of all day 5 human blastocysts using Fiji 1.53q software (Supplemental Table 1). Multi-point outlines of the external and internal embryo, inner cell mass (ICM) and blastocele cavity were drawn using the polygon tool to measure the area (µm^2), perimeter (µm), major and minor axis (µm), embryo shape and blastocele volume (Supplemental Table 1). The thickness of the zona pellucida and trophoblast (TE) cortex was measured using the line tool (Supplemental Table 1).

Evaluation of secreted proteins in spent blastocyst media

Ninety-four proteins involved in developmental programming (Supplemental Table 2) were quantified in SBM samples by proximity extension assays (PEA, Olink Development panel, Olink Proteomics). Ten microliter aliquots of SBM ($n = 32$) and control culture media ($n = 4$) were randomized in a 96-well plate. Culture media was used as blank to normalize protein levels in SBM samples. PEA combines oligonucleotide-coupled antibody recognition with the typical amplification of polymerase chain reaction (PCR). Specifically, this assay utilizes proximity-dependent DNA polymerization to generate a unique PCR target sequence indicative of the protein of interest. This sequence is then amplified and measured in real-time using a microfluidic PCR platform, maximizing the specificity and sensitivity of the assay in small sample volumes [35]. To ensure data accuracy and consistency, rigorous quality control measures included normalizing data to an internal extension control, mitigating intra-run variability, running an intra-plate control and addressing run fluctuations. Intra assays coefficient of variations (%CV) ranged from 3 to 7%. The final assay output was expressed as the normalized protein expression (NPx), and presented on a log2 scale where higher NPx values corresponded to greater protein expression levels.

Sparse Partial Least Squares Discriminant Analysis (sPLS-DA) and loading plots

Sparse Partial Least Squares Discriminant Analysis (sPLS-DA) is a supervised multivariate statistical method used to model the relationship between independent predictor variables and a categorical response variable. It extends the classical PLS-DA by incorporating

sparsity to select the most relevant variables for class discrimination. This method is particularly useful in high-dimensional datasets, where the number of variables far exceeds the number of samples. The sPLS-DA model was constructed using the mixOmics R package and splsda function [36] with 94 evaluated proteins serving as independent predictors. The categorical variable used to differentiate between groups was implantation, defined by serum b-hCG levels > 5 mIU/mL nine days after embryo transfer. A fivefold cross-validation was implemented to optimize the number of components and the number of variables to retain per component. Loading vectors, visualized with the plotLoadings function in mixOmics, were extracted from the sPLS-DA model to identify the variables contributing most to the discrimination between groups. The principal component analysis (PCA) plots illustrate the contribution of each variable to the first and second components, respectively.

Hierarchical clustering and heat map analysis

Hierarchical clustering was performed on the samples using Euclidean distance and Ward's method to generate dendrograms and visualize sample clustering. The heatmap.2 function from the gplots R package was used to generate heat maps with dendrograms [37].

Statistics analysis

Chi-square tests were used to compare categorical clinical variables (i.e., female and male indications for assisted reproductive techniques, COS protocols, blastocyst state, stage and quality, as well as the quality of the ICM and TE). The Mann–Whitney test was used to compare continuous numerical clinical variables (i.e., maternal age, duration of stimulation, the daily FSH dose, and the total FSH, hMG and LH levels during stimulation). Parametric (T-test) or non-parametric (Mann–Whitney) tests, depending on the distribution normality, were used to compare morphometric parameters and NPx values of each protein of interest. The mixOmics (6.14) and gplots (v3.1.1) R (v.4.0) packages were used to process and visualize secretomic data. Receiver operating characteristic (ROC) curves were used to assess the discriminatory power of morphometric and secretomic variables between study groups, based on the area under the curve (AUC) value [38]. Multiple regression models were built using parameters that significantly differed between groups such as internal axis ratio, roundness, circularity, and the concentration of specific protein targets (MATN2 and TMSB10) in terms of clinical outcome to evaluate the predictive capacity of these models. All statistical analyses were conducted in GraphPad Prism version 8.3.0 for Windows (GraphPad Software, Boston, Massachusetts, USA, www.graphpad.com). In all cases, $p < 0.05$ was considered statistically significant.

Results

Baseline demographics and reproductive characteristics

The maternal age, diagnosed causes of female and male infertility, cycle-associated variables (controlled ovarian stimulation [COS] protocols, hormone doses, COS duration, and fertilization techniques), transfer-associated variables (blastocyst stage, state and quality) of the whole cohort and both subgroups are presented in Table 1. The demographic and cycle-associated characteristic data were unavailable for 2/30 ICSI cycles and thus they were excluded from analysis. The mean maternal age of the cohort was 36 years. There was no significant age difference between patients that achieved implantation or not (Table 1). In this cohort, 39.28% of women had normal reproductive function while 17.85% required donor oocytes (Table 1; Supplemental Fig. 1A). Alternatively, 53.57% of men were normozoospermic and 10.71% required donor sperm (Table 1; Supplemental Fig. 1B). The distribution of indications for ICSI/ET did not significantly differ between implantation outcomes (Table 1; Supplemental Fig. 1C-D).

Regarding cycle-associated characteristics, the leading COS protocol was exclusive FSH stimulation (42.86% of cycles). 21.43% of women did not undergo COS because donor oocytes were used (Table 1; Supplemental Fig. 2A). COS protocol distribution was similar across subgroups (Supplemental Figure 2B-C), indicating there was no impact on implantation success (Table 1; Supplemental Fig. 2D-E). While there was no difference in the daily dose of FSH (Table 1; Supplemental Fig. 2F), the total FSH dose was significantly lower in patients with implantation failures (Table 1; Supplemental Fig. 2G).

In 29 out of 30 cycles, single embryo transferences (SET) were performed and only in one case two blastocysts were transferred according to clinical criteria and patient's election; both resulted in negative implantation. Most ETs involved fresh (89.29%), expanded blastocysts (85.71%), respectively (Table 1; Supplemental Fig. 3A-C). Implantation success was not significantly associated with the blastocyst stage or state (fresh or cryopreserved) (Table 1; Supplemental Fig. 3B, D). In this cohort, 50% of embryos were considered good quality (bb grade) and less than 20% were considered poor quality (35) (Table 1; Supplemental Fig. 3E). The inner cell mass was graded excellent (a) or good (b) quality in 82.14% of cases (Table 1; Supplemental Fig. 3G) whereas the trophoectoderm was considered top or good quality in 60.71% of cases and poor quality (c) in 39.29% of cases (Table 1; Supplemental Fig. 3I). No significant differences

Table 1 Comparison of baseline characteristics and clinical reproductive outcomes

Demographic characteristics	**Whole cohort** ***n*** **= 28**	**Implanted embryos** ***n*** **= 15**	**Non-implanted embryos** ***n*** **= 13**	***P*-value**	**Sig**
Maternal age (years), mean [IQR]	36 [31 - 42]	36 [31 - 42]	36 [32 - 40]	$p = 0.954$	ns
Female indication for ART, n (%)				$p = 0.483$	ns
Premature ovarian failure and cycle with donated oocytes	2 (7.14%)	0 (0%)	2 (15.38%)		
Normal reproductive function / idiopathic infertility	11 (39.28%)	5 (33.33%)	6 (46.15%)		
Premature ovarian failure	3 (10.71%)	2 (13.33%)	1 (7.69%)		
Non-obstructive tubal lesion	1 (3.57%)	0 (0%)	1 (7.69%)		
Bilateral salpingectomy / cycle with donated oocytes	1 (3.57%)	1 (6.67%)	0 (0%)		
Genetic malformation	1 (3.57%)	1 (6.67%)	0 (0%)		
Endometriosis	2 (7.14%)	1 (6.67%)	1 (7.69%)		
Endometriosis / cycle with donated oocytes	1 (3.57%)	1 (6.67%)	0 (0%)		
Anovulation	4 (14.28%)	3 (20%)	1 (7.69%)		
Cycle with donated oocytes	2 (7.14%)	1 (6.67%)	1 (7.69%)		
Male indication for ART, n (%)				$p = 0.258$	ns
Cycle with donated semen	2 (7.14%)	1 (6.67%)	1 (7.69%)		
Normozoospermia	15 (53.57%)	8 (53.33%)	7 (53.85%)		
Teratozoospermia	3 (10.71%)	1 (6.67%)	2 (15.38%)		
Criptozoospermia	3 (10.71%)	1 (6.67%)	2 (15.38%)		
Oligoteratozoospermia	1 (3.57%)	0 (0%)	1 (7.69%)		
Astenoteratozoospermia	1 (3.57%)	1 (6.67%)	0 (0%)		
Oligoastenozoospermia	1 (3.57%)	1 (6.67%)	0 (0%)		
Criptozoospermia / cycle with donated semen	1 (3.57%)	1 (6.67%)	0 (0%)		
Astenozoospermia	1 (3.57%)	1 (6.67%)	0 (0%)		
Cycle-associated characteristics					
COS protocol, n (%)				$p = 0.861$	ns
No COS	6 (21.43%)	3 (20%)	3 (23.08%)		
FSH only	12 (42.86%)	6 (40%)	6 (46.15%)		
FSH + hMG	6 (21.43%)	3 (20%)	3 (23.08%)		
FSH + LH	4 (14.29%)	3 (20%)	1 (7.69%)		
Duration of stimulation (days), mean [IQR]	11 [7 - 19]	12 [10 - 19]	10 [7 - 15]	$p = 0.115$	ns
Daily FSH dose (IU/day), mean [IQR]	264 [84—360]	290.8 [84—360]	235 [100—300]	0.053	ns
Total FSH dose during stimulation (IU), mean [IQR]	2909 [1200—4200]	3383 [1592—4200]	2340 [1200—3600]	$p = 0.005$	**
Total hMG dose during stimulation (IU), mean [IQR]	282 [0—1500]	247.9 [0—1500]	322.5 [0—1500]	$p = 0.858$	ns
Total LH dose during stimulation (IU), mean [IQR]	266 [0—2100]	350 [0—2100]	165 [0—1650]	$p = 0.444$	ns
Fertilization technique, n (%)				NA	NA
ICSI	28 (100%)	15 (100%)	13 (100%)		
Embryo state, n (%)				$p = 0.232$	ns
Fresh	25 (89.29%)	13 (86.67%)	12 (92.31%)		
Frozen	3 (10.71%)	2 (13.33%)	1 (7.69%)		
Blastocyst stage, n (%)				$p = 0.630$	ns
BC	1 (3.57%)	1 (6.67%)	0 (0%)		
BE	24 (85.71%)	13 (86.67%)	11 (84.62%)		
BHi	3 (10.71%)	1 (6.67%)	2 (15.38%)		
Quality of transferred blastocyst, n (%)				$p = 0.118$	ns
aa	1 (3.57%)	0 (0%)	1 (7.69%)		
ab	2 (7.14%)	2 (13.33%)	0 (0%)		
bb	14 (50%)	7 (46.67%)	7 (53.85%)		
bc	6 (21.43%)	5 (33.33%)	1 (7.69%)		
cc	5 (17.86%)	1 (6.67%)	4 (30.77%)		
Quality of ICM, n (%)				$p = 0.246$	ns

Table 1 (continued)

Demographic characteristics	Whole cohort *n* = 28	Implanted embryos *n* = 15	Non-implanted embryos *n* = 13	*P*-value	Sig
A	3 (10.71%)	2 (13.33%)	1 (7.69%)		
B	20 (71.43%)	12 (80%)	8 (61.54%)		
C	5 (17.86%)	1 (6.67%)	4 (30.77%)		
Quality of TE, n (%)				$p = 0.547$	ns
A	1 (3.57%)	0 (0%)	1 (7.69%)		
B	16 (57.14%)	9 (60%)	7 (53.85%)		
C	11 (39.29%)	6 (40%)	5 (38.46%)		
Clinical Outcomes					
Implantation rate, n (%)	15 (53.57%)	NA	NA	NA	
Biochemical pregnancy rate, n (%)	1 (6.67%)	NA	NA	NA	
Clinical pregnancy rate, n (%)	14 (93.33%)	NA	NA	NA	
Clinical miscarriage rate, n (%)	3 (21.43%)	NA	NA	NA	
Live birth rate, n (%)	11 (78.57%)	NA	NA	NA	

This table includes data from 28/30 cycles that had complete study data. Implantation rates were calculated considering all transfer cycles ($n = 28$). Biochemical pregnancies and clinical pregnancy rates were calculated per positive implantation cases ($n = 15$). Miscarriage and live birth rates were calculated per clinical pregnancy ($n = 14$). Chi-square tests were used to compare categorical variables (i.e., female and male indications for ART, COS protocols, blastocyst state, stage and quality, as well as the quality of the ICM and TE). The Mann–Whitney test was used to compare continuous numerical variables (i.e., maternal age, duration of stimulation, the daily FSH dose, and the total FSH, hMG and LH levels during stimulation. In all cases, *p*-values < 0.05 were considered statistically significant

IQR interquartile range, *COS* controlled ovarian stimulation, *FSH* follicle stimulating hormone, *hMG* human menopausal gonadotropin, *LH* luteinizing hormone, *IU* international units, *ET* embryo transfer, *BC* cavitated blastocyst, *BE* expanded blastocyst, *BHi* blastocyst initiating hatching, *ICM* inner cell mass, *TE* trophoectoderm, *NA* not applicable, *ns* no significant difference

$^{**}p < 0.01$

in embryo quality distribution were observed between subgroups (Table 1; Supplemental Fig. 3F, H, J).

Overall, no cycle-associated variables, COS protocols, hormone doses, SET type, or embryo quality assessments were associated with implantation success. Implantation was achieved in 53.57% of cycles leading to a clinical pregnancy rate over 90% and a live birth rate over 75%. Biochemical pregnancies accounted for 6.67% of implantations, and 21.43% of clinical pregnancies ended in miscarriage (Table 1).

Morphometric analysis of implanted versus non-implanted embryos

Forty-three morphometric parameters were measured in 32 blastocysts (Supplemental Table 3), which were homogenously subdivided according to their ability to implant. Five of the forty-three morphometric parameters were associated with significant differences between implanting and non-implanting embryos (Fig. 1; Supplemental Table 4). Notably, four out of five morphometric parameters described the shape of the embryo's internal contour, defined as the circumference with respect to the trophoblast cortex, not the zona pellucida. This suggests that embryos with a more rounded and spherical shape are more likely to implant. Specifically, internal circularity and roundness were found to be significantly higher in implanting embryos ($p < 0.01$ in both cases; Fig. 1A-B; Supplemental Table 4) whereas the internal axis ratio and angle were significantly higher in non-implanting embryos ($p < 0.05$ in both cases; Fig. 1C-D; Supplemental Table 4). Finally, implanting embryos were associated with a significantly thinner trophoblast width ($p = 0.0270$; Fig. 1E; Supplemental Table 4). With the exception of the internal angle, the individual values observed for the other four clinically-relevant morphometric parameters tended to be more dispersed for non-implanting embryos than implanting embryos (Fig. 1; Supplemental Table 4). Hence, implanting embryos showed less variation in the morphometric parameters (excluding internal angle) compared to non-implanting embryos. This suggest that implanting embryos tend to have a more spherical and rounded morphology with a thin trophoblast width, whereas non-implanting embryos showed greater variability in morphometric measurements.

Secretomic analysis of implanted versus non-implanted embryos

Out of 94 proteins analysed in SBM, 86 were quantifiable. Six proteins were excluded due to failure to be quantified in > 50% of the samples. Twelve of the thirty-two (37.5%) SBM samples had insufficient volume for PEA, leaving SBM samples from 11 (34.4%) implanting and 9 (28.1%) non-implanting embryos available for analysis. sPLS-DA revealed that most embryos with the ability to implant

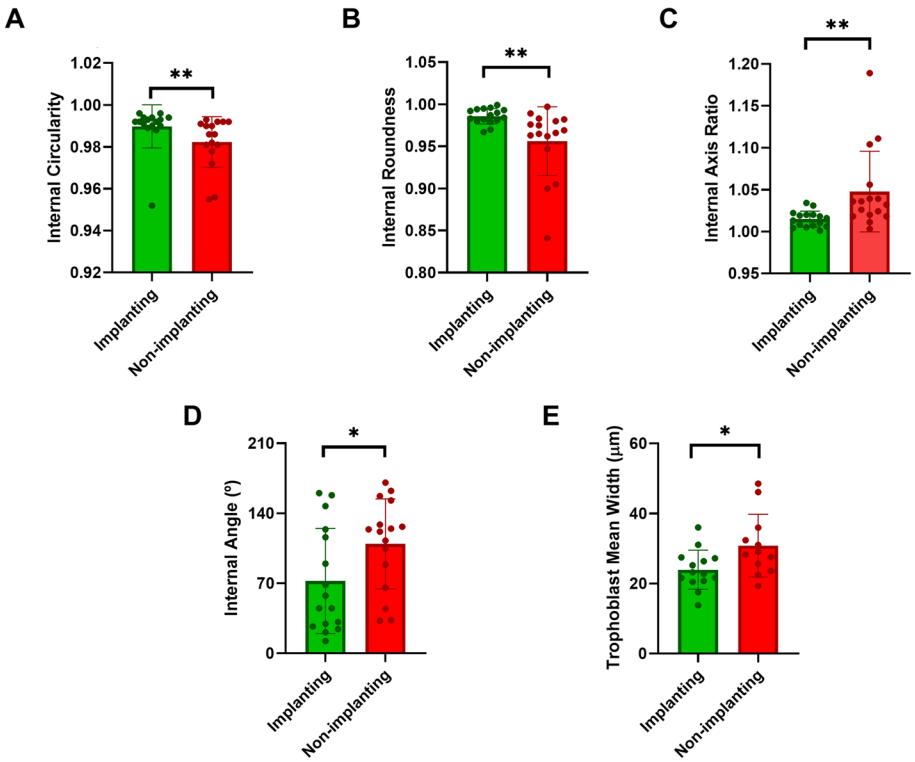

Fig. 1 Morphometric differences in implanting and non-implanting embryos. Column plots displaying day 5 embryo internal circularity (**A**) and internal roundness (**B**) expressed as ratios ranging from 0 to 1, indicating shape roughness and circle-like shape respectively. The internal axis ratio between the major and minor embryo axes (**C**) and internal angle of the best-fit elipse (**D**), and mean trophoblast width (**E**) are also presented. Morphometric measurements are defined and illustrated in Supplementary Table 1. Successful implantation was defined as a serum b-hCG levels > 5 mIU/mL nine days after embryo transfer. Data is presented as the mean ± standard deviation. Dots correspond to individual measures. Statistical differences in morphometric measurements between implanting and non-implanting embryos were evaluated with the Mann–Whitney test. *$p < 0.05$; **$p < 0.01$

(See figure on next page.)

Fig. 2 Secreted protein signature of implanted and non-implanted embryos. **A** Sparse Partial Least Squares Discriminant Analysis (sPLS-DA) showing grouping of implanted (1) and non-implanted (0) embryos based on the secreted protein profile. **B** Loading plot displaying the ten proteins highest (red) and lowest (blue) abundance in implanted (1) and non-implanted (0) embryos. **C** Logarithmic scale of raw p-values from the unpaired t-test (-log(raw.p)) for each compound. **D**-**F** Normalised protein expression of differentially secreted protein markers between implanting and non-implanting embryos. *$p < 0.05$

had a distinct secreted protein profile than embryos without the ability to implant, although there was slight overlap between groups (Fig. 2A). The top ten proteins distinguishing implantation fate are presented in Fig. 2B. Interestingly, the top three proteins related to implantation outcomes with the loading plot (Matrilin-2, MATN2; legumain, LGMN; thymosin beta-10, TMSB10) were also found to be differentially secreted by implanting and non-implanting embryos ($p < 0.05$; Fig. 2B-C). Implanting embryos secreted significantly more MATN2 and LGMN ($p < 0.01$ in both cases; Fig. 2D-E) and significantly less TMSB10 ($p < 0.05$; Fig. 2F) than non-implanting embryos.

Predicting human embryo implantation potential with morphometric and secretomic data

To develop a reliable, non-invasive method to identify embryos with the ability to implant, combinations of the five significant morphometric parameters were used to build an implantation prediction model. The internal axis ratio and internal roundness of day 5 blastocysts were more reliable image-based markers (AUC > 0.8, $p < 0.01$ in both cases; Fig. 3A-B) than internal circularity, internal angle and trophoblast mean width (AUC > 0.7, $p < 0.05$ in all cases) (Supplemental Table 5). The model combining internal axis ratio, internal roundness and internal circularity predicted the likelihood of implantation with the

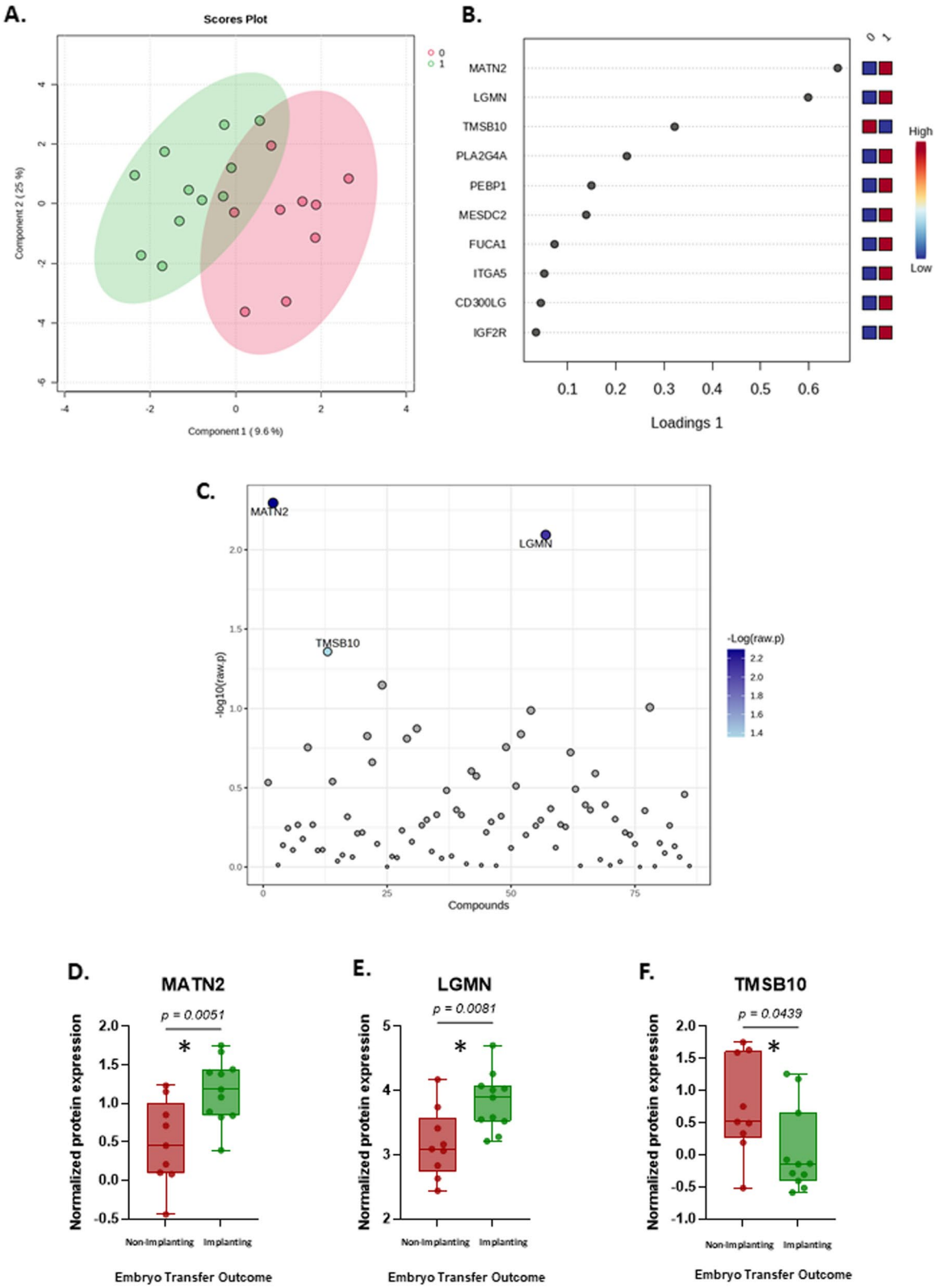

Fig. 2 (See legend on previous page.)

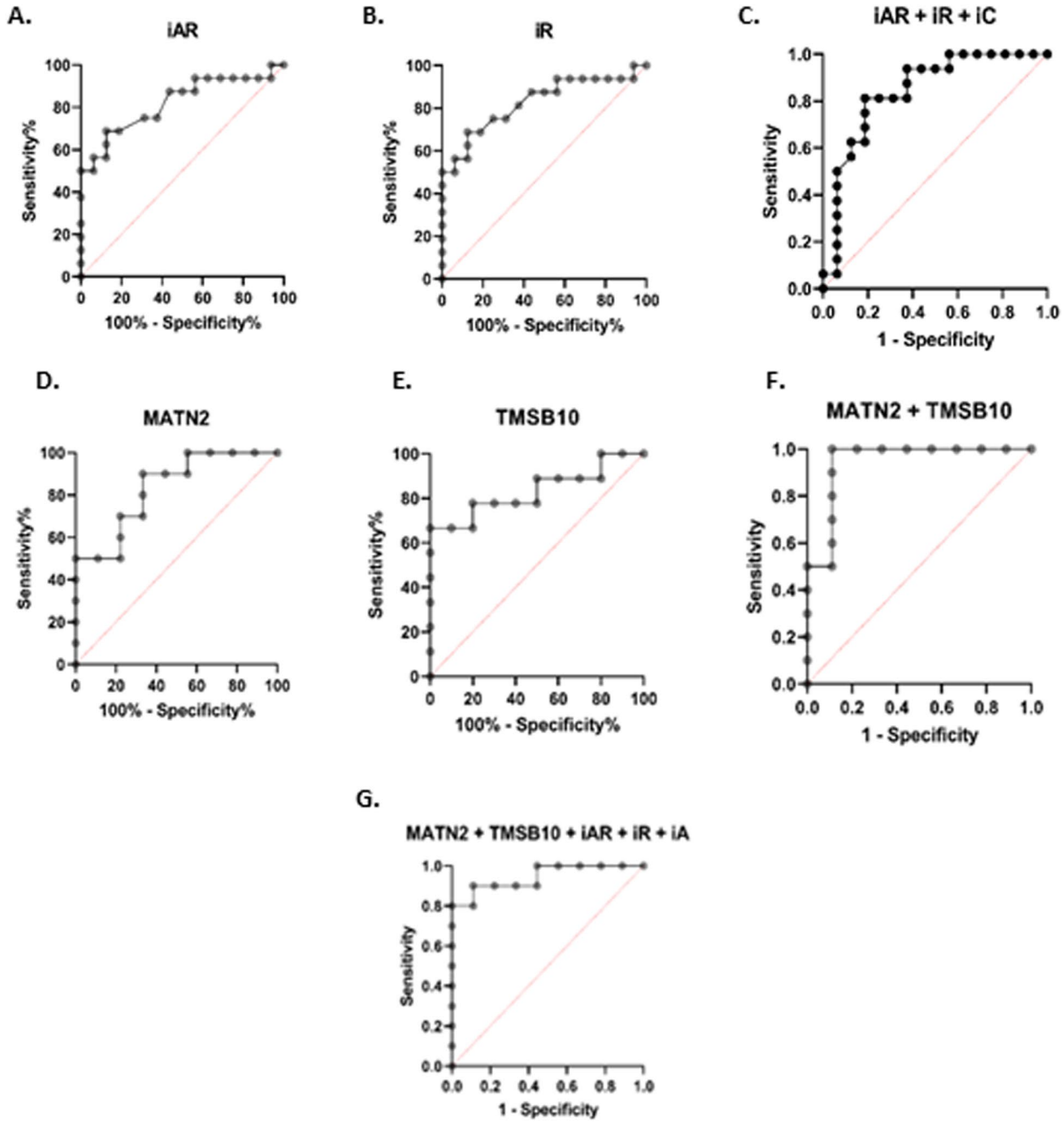

Fig. 3 Implantation predictive models based on non-invasive secretomic and/or morphometric parameters of day-5 embryos. **A**-**G** ROC curves plotting the true positive rate (sensitivity) against the false positive rate (1-specificity) to evaluate the performance of seven different implantation prediction models Embryo morphometry-based models were developed using the internal axis ratio (**A**) or internal roundness (**B**) alone, or a combination of the internal axis ratio, internal roundness and internal circularity (**C**). Similarly, embryo secretome-based models were developed using the secreted protein levels of MATN2 (**D**) and TMSB10 (**E**) alone or in combination (**F**). A model integrating five morphometric and secretomic parameters (**G**) was found to have the best performance. iA, internal angle; iAR, internal axis ratio; iR, internal roundness; iC, internal circularity; MATN2, Matrilin-2; TMSB10, thymosin beta-10

highest accuracy, with 81.25% specificity and sensitivity and an AUC of 0.8418 ($p=0.001$). The AUCs and predictive performance of the models with subpar accuracy are presented in Supplemental Table 5.

When considered individually, ROC curves highlighted MATN2 and TMBS10 as reliable predictive biomarkers of embryo implantation (AUC > 0.8, $p < 0.05$ in both cases; Fig. 3D-E), whereas LGMN alone was a fair biomarker (AUC = 0.7333, $p = 0.08$; Supplemental Table 5). Further, multiple logistic regression models showed that combining secreted MATN2 and TMSB10 protein levels efficiently discriminated implanting and non-implanting embryos (AUC = 0.94, $p < 0.01$; Fig. 3F) while models based on other secreted marker combinations did not accurately predict the likelihood of implantation (Supplemental Table 5).

Remarkably, a model integrating MATN2 and TMSB10 secreted protein levels with morphometric parameters (i.e., internal axis ratio, internal roundness and internal circularity) was able to predict implantation failure with 100% accuracy and implantation success with 90.91% accuracy (AUC = 0.9333, $p = 0.0015$; Fig. 3G; Supplemental Table 5). These findings highlighted the untapped potential of these non-invasive biomarkers. According to our results, the combination of increased MATN levels, reduced TMSB10 secretion and three key cell shape descriptors (internal axis ratio, roundness and angle) yielded the most accurate non-invasive signature for predicting implantation likelihood in our cohort.

Discussion

Our study highlights the clinical utility of embryo morphometry and the secretomic profile of spent blastocyst medium, identifying five non-invasive biomarkers of human implantation potential.

Notable limitations of gold-standard embryo morphological assessments are the potential inter-observer biases, subjective nature, and broad grading categories. Leveraging embryo morphometrics is a promising strategy to overcome these limitations [39], as granular, quantifiable data can be objectively collected from a wide range of parameters [40]. The present study reports the largest set of morphometric parameters evaluated in implanted and non-implanted blastocysts. A total of five morphometric parameters—four related to the internal shape of the embryo and one to the trophoblast thickness—were found to differ significantly between implanting and non-implanting embryos. Embryo shape descriptors like internal circularity, roundness, and axis ratio were found to be the most reliable morphometric predictors of implantation (AUC: 0.7852, 0.8262, and 0.8203, respectively).

Our results align with previous studies reporting enhanced predictive power of embryo morphometry in cleavage-stage embryos [32, 33, 40] and blastocysts [39, 41–46] compared to classical morphology grading. Most studies performing morphometric-based evaluation to assess embryo implantation potential [40, 41, 43, 45–47] and pregnancy rates [39, 44] corroborate that increased embryo and ICM area are associated with implantation and pregnancy success. Despite neither of these two parameters significantly differing among our subgroups of implanting and non-implanting blastocysts, implanting blastocysts tended to have a slightly larger external embryo area. Conversely, the similar ICM sizes observed between subgroups may have been because more than 70% of the embryos had a good quality ICM according to the ASEBIR criteria. Similarly, more than 95% of blastocysts in our cohort were either expanded (85.71%) or had initiated hatching (10.71%), which could explain why the blastocele cavity measurements, which are directly associated with expansion degree, were found to be similar regardless of the implantation fate. In contrast, 40% of the embryos in the whole cohort exhibited poor trophoblast quality. Although morphological-based assessment of trophoblast quality was not related to implantation potential, our morphometric analysis associated thinner trophoblast width with a higher likelihood of implantation; thus, indicating that this trophoblast-associated morphometric parameter depicts more accurately the role of trophoblast features in implantation success.

Many studies have overlooked cell shape descriptors [39–47]. Here, we showed that internal embryo shape was markedly different between embryos that implanted or not, supporting that round, spherical embryos with a thinner trophoblast cortex are more likely to implant. This observation aligns with the findings of our previous study, where increased embryo roundness in cleavage-stage embryos was associated with higher implantation potential [33].

Most studies proposing morphometry-based embryo assessment [39–47] or morphokinetic evaluations of time-lapse images [48–54] for embryo selection often fail to combine image-based assessments with non-invasive markers that reliably reflect embryo physiology. Here, we overcame this limitation by evaluating the embryo secretome with a set of 94 proteins involved in developmental programming. One of the major strengths of this study is the implementation of PEA technology to overcome the typical limitations inherent to classical proteomic approaches as mass spectrometry (MS), which are constrained by the limited sample volume available [55, 56]. Besides, PEA technology has already demonstrated high sensitivity and specificity in detecting low-abundance proteins, making it a powerful tool biomarker discovery [35, 57].

The BSM highlighted three embryo-derived proteins (Matrilin-2 [MATN2], legumain [LGMN], and thymosin beta 10 [TMSB10]) which were differentially secreted by implanting versus non-implanting blastocysts. The

three-protein signature effectively discriminated embryos according to their implantation potential. The most accurate negative and positive implantation prediction models were obtained when either combined secreted protein levels of MATN2 and TMSB10 or the set of three proteins (MATN2, LGMN, TMSB10). In our cohort, blastocysts were most likely to implant when they oversecreted MATN2, a multi-adhesion adaptor protein interacting with different extracellular matrix proteins [58], and the protease LGMN [59], but diminished TMSB10, a protein involved in cell proliferation and cancer progression. Exacerbated secretion of proteins involved in extracellular matrix communication such as MATN2 might contribute to the profound tissue remodelling and embryo invasion into the maternal endometrium during later phases of implantation [60, 61]. In addition to role of MATN2 in tissue remodelling at the embryo-maternal interface, there is evidence of MATN2 mediating inflammatory processes [62]. Thus, embryo-derived MATN2 may contribute to the pro-inflammatory environment that is required for embryo implantation [63, 64]. Similarly, the secretion of proteases such as LGMN [59] could be hypothesized to support the embryo-endometrial crosstalk by allowing the implanting embryo to participate in remodelling the endometrial niche for a successful invasion [59, 65]. Finally, TMSB10 has an established role in promoting cell proliferation during cancer progression [66–68], but its implication in embryo development and implantation-related processes remains unexplored. Implanting blastocysts secreting lower levels of TMSB10 may be experiencing a shift in the cell proliferation/differentiation balance that promotes embryo cell lineage differentiation, while non-implanting embryos may be proliferating beyond control. However, this assumption requires further functional studies. Noteworthily, although the molecular functions of the three protein targets align with the embryo implantation process, there is a possibility that these proteins are downstream effects rather than drivers of implantation. This is supported by studies in animal models, which have not reported gross abnormalities in knock-out mice [69]. Hence, while their differential expression in implanting versus non-implanting blastocysts is a significant finding, it does not definitively establish a causal link. It is equally plausible that these proteins serve as markers or downstream effects of other processes driving successful implantation. The hypothetical roles of the secreted markers identified in this study in the implantation mechanism should be validated trough larger-scale in-vitro or in-vivo experiments.

A major limitation of the current pilot study is the limited sample size, which can lead to the curse of dimensionality. To address this challenge, several strategies were employed. Initially, image-based features were compared individually between groups. For the analysis of the 94 secreted proteins, sparse Partial Least Squares Discriminant Analysis (sPLS-DA) was implemented. sPLS-DA mitigates the curse of dimensionality by perfoming dimension reduction and feature selection, creating latent variables that capture the most relevant information while reducing the number of variables in the model. This approach minimizes overfitting, improves computational efficiency, and addresses multicollinearity. Subsequent models and ROC curve analyses were constructed using only the significant image-based and secreted protein parameters, resulting in streamlined models based on individual or a limited number of significant key parameters.

Despite the efforts to overcome the challenges of analyzing high-dimensional data, it is crucial to acknowledge that the small sample size restricts the scope of this study to a small-scale interpretation. While the results are promising, the limited sample size and the fact that this is a single-center study mean that the findings should be viewed as preliminary exploration of a potential non-invasive signature. Further validation in larger and independent cohorts is needed to confirm our results.

Morphometric parameter measurement, easily performed using open-source software like Fiji, can be further automated using AI tools to minimize operator error. The objective and quantitative nature of morphometric assessment offers significant advantages over traditional qualitative morphological evaluations. Additionally, commercially available proximity-based assays enable rapid protein quantification delivering results in under two hours with minimal hands-on time. Once the key protein targets (MATN2, LGMN, and TMSB10) identified in this study are validated, the next step will be to develop individual proximity-based immunoassays for these markers. The integration of this image-based and secreted protein signature could allow implantation potential predictions within 2–3 h of embryo evaluation, making it feasible for same-day assesment at embryo transfer, enhancing its clinical potential. In conclusion, this work represents a step forward in the field of non-invasive embryo selection, combining a signature of secreted proteins with a morphometric profile associated to likelihood of implantation. Our predictive model provides a reliable alternative for clinics without time-lapse systems or access to preimplantation genetic testing.

Supplementary Information

The online version contains supplementary material available at https://doi.org/10.1186/s12958-025-01386-z.

Supplementary Material 1: Supplementary Table 1. Descriptions of morphometric parameters in day 5 blastocysts.

Supplementary Material 2: Supplementary Table 2. All measured proteins included in the Development Panel (Olink Proteomics).

Supplementary Material 3: Supplementary Figure 1. Etiology of infertility in our study population. Pie charts showing reproductive function/cycle types in female (A) and male (B) participants with complete study data. (C-D) Chi-square tests found no statistical differences ($p > 0.05$) between subgroups of patients who achieved implantation or not. DO, donated oocytes; DS, donated sperm; NRF, normal reproductive function.

Supplementary Material 4: Supplementary Figure 2. Comparison of implantation outcomes based on controlled ovarian stimulation (COS) protocols. Pie charts showing the proportion of COS protocol types in all IVF cycles (A), and subgroups of patients with positive (B) and negative (C) implantation outcomes. (D) Chi-squared tests showed no statistical differences in implantation outcomes based on COS protocols ($p > 0.05$). Violin plots depicting the (E) duration of COS protocols and (F) daily dose of FSH. Box and whiskers plots depicting the total doses of FSH (G), hMG (H) and LH (I) administered during COS. Data are presented as the mean ± standard deviation. The Mann–Whitney test was used to compare the duration of stimulation, daily FSH dose, as well as the total FSH, hMG and LH administered during COS. COS, controlled ovarian stimulation; FSH, follicle stimulating hormone; hMG, human menopausal gonadotropin; LH, luteinizing hormone; IU, international units. ns: no statistically significant differences. $^{**}p < 0.01$.

Supplementary Material 5: Supplementary Figure 3. Comparison of implantation outcomes based on embryo stage, quality and state. Pie charts showing the proportion of (A) cavitated blastocysts (BC), expanded blastocysts (BE), blastocysts that initiated hatching (Bhi) by day 5; (C) fresh or cryopreserved blastocysts; (E) embryo, (G) inner cell mass (ICM), and (I) trophectoderm (TE) quality graded using the ASEBIR criteria, with "a" representing top quality and "c" representing poor quality. Note, the first letter of the embryo grading refers to the inner cell mass grade whereas the second letter refers to trophectoderm grade. (B, D, F, H, J) Chi-square tests showed implantation outcomes were not statistically different based on blastocyst stage, state, and quality ($p > 0.05$ in all cases). ns, no statistically significant differences.

Supplementary Material 6: Supplementary Table 3. Descriptive statistics of morphometric parameters.

Supplementary Material 7: Supplemental Table 4. Comparison of morphometric measurements in implanting and non-implanting day 5 blastocysts.

Supplementary Material 8: Supplemental Table 5. Comparison of the predictive performance of models based on morphometric and/or secretomic markers.

Authors' contributions

A.P. and R.Y.S. equally conducted the experiments and contributed to data curation, formal analysis, investigation, methodology, visualization and writing – original draft, review and editing. J.V.M.S, I.I, P.J.F.C. A.M. and J.M.R. participated in investigation. A.Q. participated in investigation and methodology. I.M. conceptualized the study and contributed to data curation, investigation, methodology, supervision and writing – review and editing. F.D. participated in conceptualization and was responsible for funding acquisition, investigation, methodology, project administration, resources, supervision and writing – original draft, review and editing. All authors actively contributed to critical revision and manuscript editing in its final form.

Funding

This research was funded by the Institute of Health Carlos III (ISCIII) (Spanish Ministry of Science and Innovation) through the FIS program granted to F.D. (PI20/00405 and PI23/00860), co-funded by the European Union, and the Generalitat Valenciana through the Grant Program for Consolidated Research Groups (CIAICO/2022/203 [F.D.]), Grant for the hiring of support staff linked to a technology transfer project (CIAPOT/2022/18 [A.P.] and CIACIF/2021/051 [R.Y.-S.]).

Data availability

No datasets were generated or analysed during the current study.

Declarations

Ethics approval and consent to participate

Ethical Research Board of the Polytechnic University Hospital La Fe approved this research under the reference number 2018/0669. All participants provided written informed consent prior to their inclusion.

Consent for publication

Not applicable.

Competing interests

The authors declare no competing interests.

Author details

[1]IVIRMA Global Research Alliance, IVI Foundation, Instituto de Investigación Sanitaria La Fe (IIS La Fe), Valencia 46026, Spain. [2]Unit of Assisted Reproduction, Hospital Universitario y Politécnico La Fe, Valencia 46026, Spain. [3]Stanford Medicine School, Ob Gyn Department, Stanford University, Stanford, CA 94304, USA. [4]Fundación Instituto Valenciano de Infertilidad, Instituto de Investigación Sanitaria La Fe, Edificio Biopolo, Torre A, Planta 1, Avenida Fernando Abril Martorell, 106, Valencia 46026, Spain.

Received: 17 December 2024 Accepted: 18 March 2025
Published online: 12 April 2025

References

1. Hollywood K, Brison DR, Goodacre R. Metabolomics: Current technologies and future trends. Proteomics. 2006;6(17):4716–23. https://doi.org/10.1002/pmic.200600106.
2. Seli E, Sakkas D, Scott R, Kwok SC, Rosendahl SM, Burns DH. Noninvasive metabolomic profiling of embryo culture media using Raman and near-infrared spectroscopy correlates with reproductive potential of embryos in women undergoing in vitro fertilization. Fertil Steril. 2007;88:1350–7. Available from: https://www.fertstert.org/article/S0015-0282(07)03049-X/pdf. Cited 2019 Apr 10.
3. Butler SA, Luttoo J, Freire MOT, Abban TK, Borrelli PTA, Iles RK. Human chorionic gonadotropin (hCG) in the secretome of cultured embryos: hyperglycosylated hCG and hCG-Free beta subunit are potential markers for infertility management and treatment. Reprod Sci. 2013;20:1038–45.
4. Mains LM, Christenson L, Yang B, Sparks AET, Mathur S, Van Voorhis BJ. Identification of apolipoprotein A1 in the human embryonic secretome. Fertil Steril. 2011;96:422-427.e2.
5. Noci I, Fuzzi B, Rizzo R, Melchiorri L, Criscuoli L, Dabizzi S, et al. Embryonic soluble HLA-G as a marker of developmental potential in embryos. Hum Reprod. 2005;20:138–46.
6. Saith RR, Bersinger NA, Barlow DH, Sargent IL. The role of pregnancy-specific -1 glycoprotein (SP1) in assessing human blastocyst quality in vitro. Hum Reprod. 1996;11:1038–42.
7. Alegre L, Del Gallego R, Arrones S, Hernández P, Muñoz M, Meseguer M. Novel noninvasive embryo selection algorithm combining time-lapse morphokinetics and oxidative status of the spent embryo culture medium. Fertil Steril. 2019;111:918-927.e3.
8. Dominguez F, Meseguer M, Aparicio-Ruiz B, Piqueras P, Quiñonero A, Simón C. New strategy for diagnosing embryo implantation potential by combining proteomics and time-lapse technologies. Fertil Steril. 2015;104:908–14.
9. Tejera A, Castelló D, de Los Santos JM, Pellicer A, Remohí J, Meseguer M. Combination of metabolism measurement and a time-lapse system provides an embryo selection method based on oxygen uptake and chronology of cytokinesis timing. Fertil Steril. 2016;106:119-126.e2.
10. Borges E, Braga DPAF, Setti AS, Montanni DA, Cabral EC, Eberlin MN, et al. Non-invasive prediction of blastocyst implantation, ongoing pregnancy

and live birth, by mass spectrometry lipid fingerprinting. J Bras Reprod Assist. 2016;20:227–31.
11. Braga DP de AF, Setti AS, Cabral EC, Eberlin M, Loturco EG, Borges E. Non-invasive prediction of blastocyst formation by day three embryo culture medium mass spectrometry lipid fingerprinting. J Bras Reprod Assist. 2015;19:119–24.
12. Feichtinger M, Vaccari E, Carli L, Wallner E, Mädel U, Figl K, et al. Non-invasive preimplantation genetic screening using array comparative genomic hybridization on spent culture media: a proof-of-concept pilot study. Reprod Biomed Online. 2017;34:583–9.
13. Rubio C, Navarro-Sánchez L, García-Pascual CM, Ocali O, Cimadomo D, Venier W, et al. Multicenter prospective study of concordance between embryonic cell-free DNA and trophectoderm biopsies from 1301 human blastocysts. Am J Obstet Gynecol. 2020;223:751.e1-751.e13.
14. Rubio C, Rienzi L, Navarro-Sánchez L, Cimadomo D, García-Pascual CM, Albricci L, et al. Embryonic cell-free DNA versus trophectoderm biopsy for aneuploidy testing: concordance rate and clinical implications. Fertil Steril. 2019;112:510–9.
15. Liu W, Liu J, Du H, Ling J, Sun X, Chen D. Non-invasive pre-implantation aneuploidy screening and diagnosis of beta thalassemia IVSII654 mutation using spent embryo culture medium. Ann Med. 2017;49:319–28.
16. Balaguer N, Rodrigo L, Mateu-Brull E, Campos-Galindo I, Castellón JA, Al-Asmar N, et al. Non-invasive cell-free DNA-based approach for the diagnosis of clinical miscarriage: A retrospective study. BJOG. 2024;131:213–21.
17. Ferrick L, Lee YS, Gardner DK. Reducing time to pregnancy and facilitating the birth of healthy children through functional analysis of embryo physiology†. Biol Reprod. 2019;101(6):1124–39.
18. Gardner DK, Meseguer M, Rubio C, Treff NR. Diagnosis of human preimplantation embryo viability. Hum Reprod Update. 2015;21:727–47.
19. Assarsson E, Lundberg M, Holmquist G, Björkesten J, Bucht Thorsen S, Ekman D, et al. Homogenous 96-Plex PEA immunoassay exhibiting high sensitivity, specificity, and excellent scalability. Hoheisel JD, editor. PLoS One. 2014;9:e95192.
20. Lundberg M, Eriksson A, Tran B, Assarsson E, Fredriksson S. Homogeneous antibody-based proximity extension assays provide sensitive and specific detection of low-abundant proteins in human blood. Nucleic Acids Res. 2011;39:e102–e102.
21. Berggrund M, Enroth S, Lundberg M, Assarsson E, Stålberg K, Lindquist D, et al. Identification of candidate plasma protein biomarkers for cervical cancer using the multiplex proximity extension assay. Molecular & Cellular Proteomics. 2019;18:mcp.RA118.001208. Available from: http://www.ncbi.nlm.nih.gov/pubmed/30692274. Cited 2019 Apr 8.
22. Jabbari E, Woodside J, Guo T, Magdalinou NK, Chelban V, Athauda D, et al. Proximity extension assay testing reveals novel diagnostic biomarkers of atypical parkinsonian syndromes. J Neurol Neurosurg Psychiatry. 2019;jnnp-2018–320151. Available from: http://www.ncbi.nlm.nih.gov/pubmed/30867224. Cited 2019 Apr 8.
23. Kasaian MT, Lee J, Brennan A, Danto SI, Black KE, Fitz L, et al. Proteomic analysis of serum and sputum analytes distinguishes controlled and poorly controlled asthmatics. Clin Exper Allergy. 2018;48:814–24. Available from: http://www.ncbi.nlm.nih.gov/pubmed/29665127. Cited 2019 Apr 8.
24. Kulasingam A, Hvas AM, Grove EL, Funck KL, Kristensen SD. Detection of biomarkers using a novel proximity extension assay in patients with ST-elevation myocardial infarction. Thromb Res. 2018;172:21–8. Available from: http://www.ncbi.nlm.nih.gov/pubmed/30343179. Cited 2019 Apr 8.
25. Lareyre F, Moratal C, Chikande J, Jean-Baptiste E, Hassen-Khodja R, Neels J, et al. Investigation of plasma inflammatory profile in diabetic patients with abdominal aortic aneurysm: a pilot study. Vasc Endovascular Surg. 2018;52:597–601. Available from: http://www.ncbi.nlm.nih.gov/pubmed/29940819. Cited 2019 Apr 8.
26. Lind L, Ärnlöv J, Lindahl B, Siegbahn A, Sundström J, Ingelsson E. Use of a proximity extension assay proteomics chip to discover new biomarkers for human atherosclerosis. Atherosclerosis. 2015;242:205–10. Available from: http://www.ncbi.nlm.nih.gov/pubmed/26204497. Cited 2019 Apr 8.
27. Petrackova A, Smrzova A, Gajdos P, Schubertova M, Schneiderova P, Kromer P, et al. Serum protein pattern associated with organ damage and lupus nephritis in systemic lupus erythematosus revealed by PEA immunoassay. Clin Proteomics. 2017;14:32. Available from: http://www.ncbi.nlm.nih.gov/pubmed/29026368. Cited 2019 Apr 8.
28. Santema BT, Kloosterman M, Van Gelder IC, Mordi I, Lang CC, Lam CSP, et al. Comparing biomarker profiles of patients with heart failure: atrial fibrillation vs sinus rhythm and reduced vs preserved ejection fraction. Eur Heart J. 2018;39:3867–75. Available from: http://www.ncbi.nlm.nih.gov/pubmed/30137304.
29. Bori L, Dominguez F, Fernandez EI, Del Gallego R, Alegre L, Hickman C, et al. An artificial intelligence model based on the proteomic profile of euploid embryos and blastocyst morphology: a preliminary study. Reprod Biomed Online. 2021;42:340–50.
30. Bori L, Meseguer F, Valera MA, Galan A, Remohi J, Meseguer M. The higher the score, the better the clinical outcome: retrospective evaluation of automatic embryo grading as a support tool for embryo selection in IVF laboratories. Hum Reprod. 2022;37:1148–60.
31. Lindgren KE, Gülen Yaldir F, Hreinsson J, Holte J, Kårehed K, Sundström-Poromaa I, et al. Differences in secretome in culture media when comparing blastocysts and arrested embryos using multiplex proximity assay. Ups J Med Sci. 2018;123:143–52.
32. Molina I, Lázaro-Ibáñez E, Pertusa J, Debón A, Martínez-Sanchís JV, Pellicer A. A minimally invasive methodology based on morphometric parameters for day 2 embryo quality assessment. Reprod Biomed Online. 2014;29(4):470–80.
33. Molina I, Martínez JV, Pertusa JF, Balasch S, Iniesta I, Pellicer A. Assessment of the implantation of day-2 human embryos by morphometric nonsubjective parameters. Fertil Steril. 2014;102:1022–8.
34. Cuevas Saiz I, Carme Pons Gatell M, Vargas MC, Delgado Mendive A, Rives Enedáguila N, Moragas Solanes M, et al. The Embryology Interest Group: updating ASEBIR's morphological scoring system for early embryos, morulae and blastocysts. Medicina Reproductiva y Embriología Clínica. 2018;5:42–54.
35. Assarsson E, Lundberg M, Holmquist G, Björkesten J, Thorsen SB, Ekman D, et al. Homogenous 96-plex PEA immunoassay exhibiting high sensitivity, specificity, and excellent scalability. PLoS One. 2014;9:e95192.
36. Rohart F, Gautier B, Singh A, Lê Cao KA. mixOmics: An R package for 'omics feature selection and multiple data integration. PLoS Comput Biol. 2017;13(11):e1005752.
37. Key M. A tutorial in displaying mass spectrometry-based proteomic data using heat maps. BMC Bioinformatics. 2012;13:1–3.
38. Muller MP, Tomlinson G, Marrie TJ, Tang P, McGeer A, Low DE, et al. Can routine laboratory tests discriminate between severe acute respiratory syndrome and other causes of community-acquired pneumonia? Clin Infect Dis. 2005;40:1079–86.
39. Utsuno H, Ishimaru T, Matsumoto M, Sasamori C, Takahashi H, Kimura H, et al. Morphometric assessment of blastocysts: relationship with the ongoing pregnancy rate. F and S Reports. 2023;4:4.
40. Alhelou Y, Hamdan M, Razali N, Adenan N, Ali J. Novel image analyser-assisted morphometric methodology offer unique opportunity for selection of embryos with potential for implantation. BMC Pregnancy Childbirth. 2023;23(1):698.
41. Roudebush WE, Williams SE, Forstein DA, Lessey BA, Likes CE, Miller PB. Predicting implantation potential using morphometric analysis of blastocysts and calculating for phi to determine a reference point. Fertil Steril. 2014;102(3):e308.
42. Gui B, Yao Z, Huang Y, Mei L, Li Y, Liu D, et al. Morphometric analysis and developmental comparison of embryos from carriers with balanced chromosomal rearrangements in preimplantation genetic diagnosis cycles. Reprod Fertil Dev. 2016;28:1953–63.
43. Chavez-Badiola A, Flores-Saiffe Farias A, Mendizabal-Ruiz G, Garcia-Sanchez R, Drakeley AJ. Development and preliminary validation of an automated static digital image analysis system utilizing machine learning for blastocyst selection. Fertil Steril. 2019;112:e149-50.
44. Sciorio R, Thong D, Thong KJ, Pickering SJ. Clinical pregnancy is significantly associated with the blastocyst width and area: a time-lapse study. J Assist Reprod Genet. 2021;38:847–55.
45. Lagalla C, Barberi M, Orlando G, Sciajno R, Bonu MA, Borini A. A quantitative approach to blastocyst quality evaluation: morphometric analysis and related IVF outcomes. J Assist Reprod Genet. 2015;32:705–12.
46. Sciorio R, Campos G, Palini S, Baldini D, Janssens R. Real-time image and time-lapse technology to select the single blastocyst to transfer in assisted reproductive cycles. Zygote. 2023;31(3):207–16.
47. Fruchter-Goldmeier Y, Kantor B, Ben-Meir A, Wainstock T, Erlich I, Levitas E, et al. An artificial intelligence algorithm for automated blastocyst

morphometric parameters demonstrates a positive association with implantation potential. Sci Rep. 2023;13:13.
48. Payá E, Bori L, Colomer A, Meseguer M, Naranjo V. Automatic characterization of human embryos at day 4 post-insemination from time-lapse imaging using supervised contrastive learning and inductive transfer learning techniques. Comput Methods Programs Biomed. 2022;221:106895.
49. Paya E, Pulgarín C, Bori L, Colomer A, Naranjo V, Meseguer M. Deep learning system for classification of ploidy status using time-lapse videos. F and S Sci. 2023;4:211–8.
50. Bori L, Meseguer F, Valera MA, Galan A, Remohi J, Meseguer M. The higher the score, the better the clinical outcome: Retrospective evaluation of automatic embryo grading as a support tool for embryo selection in IVF laboratories. Human Reprod. 2022;37:1148–60.
51. Alegre L, Del Gallego R, Bori L, Loewke K, Maddah M, Aparicio-Ruiz B, et al. Assessment of embryo implantation potential with a cloud-based automatic software. Reprod Biomed Online. 2021;42(1):66–74.
52. Barnes J, Brendel M, Gao VR, Rajendran S, Kim J, Li Q, et al. A non-invasive artificial intelligence approach for the prediction of human blastocyst ploidy: a retrospective model development and validation study. Lancet Digit Health. 2023;5(1):e28–40.
53. Meseguer M, Herrero J, Tejera A, Hilligsøe KM, Ramsing NB, Remoh J. The use of morphokinetics as a predictor of embryo implantation. Hum Reprod. 2011;26(10):2658–71.
54. Bartolacci A, Canto MD, Guglielmo MC, Mura L, Brigante C, Renzini MM, et al. Early embryo morphokinetics is a better predictor of post-ICSI live birth than embryo morphology: speed is more important than beauty at the cleavage stage. Zygote. 2021;29(6):495–502.
55. Waury K, de Wit R, Verberk IM, Teunissen CE, Abeln S. Deciphering protein secretion from the brain to Cerebrospinal Fluid for Biomarker Discovery. J Proteome Res. 2023;22(9):3068–80.
56. Beutgen VM, Shinkevich V, Pörschke J, Meena C, Steitz AM, Pogge von Strandmann E, et al. Secretome analysis using Affinity Proteomics and Immunoassays: a focus on Tumor Biology. Molecular and Cellular Proteomics. 2024;23:100830.
57. Lundberg M, Eriksson A, Tran B, Assarsson E, Fredriksson S. Homogeneous antibody-based proximity extension assays provide sensitive and specific detection of low-abundant proteins in human blood. Nucleic Acids Res. 2011;39(15):e102-.
58. Korpos É, Deák F, Kiss I. Matrilin-2, an extracellular adaptor protein, is needed for the regeneration of muscle, nerve and other tissues. Neural Regen Res. 2015;10(6):866–9.
59. Khan SU, Khan IM, Khan MU, Ud Din MA, Khan MZ, Khan NM, et al. Role of LGMN in tumor development and its progression and connection with the tumor microenvironment. Front Mol Biosci. 2023;7(10):1121964. https://doi.org/10.3389/fmolb.2023.1121964.
60. Ji S, Gumina D, McPeak K, Moldovan R, Post MD, Su EJ. Human placental villous stromal extracellular matrix regulates fetoplacental angiogenesis in severe fetal growth restriction. Clin Sci. 2021;135(9):1127–43.
61. O'Connor BB, Pope BD, Peters MM, Ris-Stalpers C, Parker KK. The role of extracellular matrix in normal and pathological pregnancy: future applications of microphysiological systems in reproductive medicine. Exp Biol Med. 2020;245(13):1163–74.
62. Jonas A, Thiem S, Kuhlmann T, Wagener R, Aszodi A, Nowell C, et al. Axonally derived matrilin-2 induces proinflammatory responses that exacerbate autoimmune neuroinflammation. J Clin Investig. 2014;124(11):5042–56.
63. Sehring J, Jeelani R. Human implantation: The complex interplay between endometrial receptivity, inflammation, and the microbiome. Placenta. 2022;117:179–86.
64. Dekel N, Gnainsky Y, Granot I, Racicot K, Mor G. The role of inflammation for a successful implantation. Am J Reprod Immunol. 2014;72(2):141–7.
65. Jamwal S, Jena MK, Tyagi N, Kancharla S, Kolli P, Mandadapu G, et al. Proteomic approaches to unravel the molecular dynamics of early pregnancy in farm animals: an In-Depth review. J Dev Biol. 2024;12(1):2.
66. Li Z, Li Y, Tian Y, Li N, Shen L, Zhao Y. Pan-cancer analysis identifies the correlations of Thymosin Beta 10 with predicting prognosis and immunotherapy response. Front Immunol. 2023;14:14.
67. Zhang X, Ren D, Guo L, Wang L, Wu S, Lin C, et al. Thymosin beta 10 is a key regulator of tumorigenesis and metastasis and a novel serum marker in breast cancer. Breast Cancer Res. 2017;19:1–5.
68. Xiao R, Shen S, Yu Y, Pan Q, Kuang R, Huang H. TMSB10 promotes migration and invasion of cancer cells and is a novel prognostic marker for renal cell carcinoma. Int J Clin Exp Pathol. 2019;12:305.
69. Mátés L, Nicolae C, Mörgelin M, Deák F, Kiss I, Aszódi A. Mice lacking the extracellular matrix adaptor protein matrilin-2 develop without obvious abnormalities. Matrix Biol. 2004;23(3):195–204.

Publisher's Note